
Article:
Mandal, S., Sarkar, B. orcid.org/0000-0002-4196-1225, Igalavithana, A.D. et al. (4 more authors) (2017) Mechanistic insights of 2,4-D sorption onto biochar: Influence of feedstock materials and biochar properties. Bioresource Technology, 246. pp. 160-167. ISSN 0960-8524

https://doi.org/10.1016/j.biortech.2017.07.073

Mechanistic insights of 2,4-D sorption onto biochar: Influence of feedstock materials and biochar properties

Sanchita Mandal[1], Binoy Sarkar[1,2], Avanthi Deshani Igalavithana[3], Yong Sik Ok[3,6], Xiao Yang[3], Enzo Lombi[1], and Nanthi Bolan[4,5*]

[1]Future Industries Institute (FII), University of South Australia, Mawson Lakes, SA 5095, Australia,

[2]Department of Animal and Plant Sciences, The University of Sheffield, Sheffield, S10 2 TN, UK

[3]Korea Biochar Research Center, Kangwon National University, Chuncheon 24341, Korea

[4]Cooperative Research Centre for Contaminant Assessment and Remediation of the Environment (CRC CARE), Mawson Lakes, SA 5095, Australia

[5]Global Center for Environmental Remediation, University of Newcastle, Callaghan, NSW 2308, Australia

[6]O-Jeong Eco-Resilience Institute (OJERI) & Division of Environmental Science and Ecological Engineering, Korea University, Seoul, Korea

[*]Corresponding author

Prof Nanthi Bolan

University of Newcastle

Email: Nanthi.Bolan@newcastle.edu.au

Tel: +61 2 49138750

Highlights

1. Steam activated tea waste biochar sorbed the highest amount of 2,4-D
2. Steam activation increased biochar surface area and conserved oxygen-containing functional groups
3. 2,4-D desorption was lowest in steam activated biochar

Graphical abstract

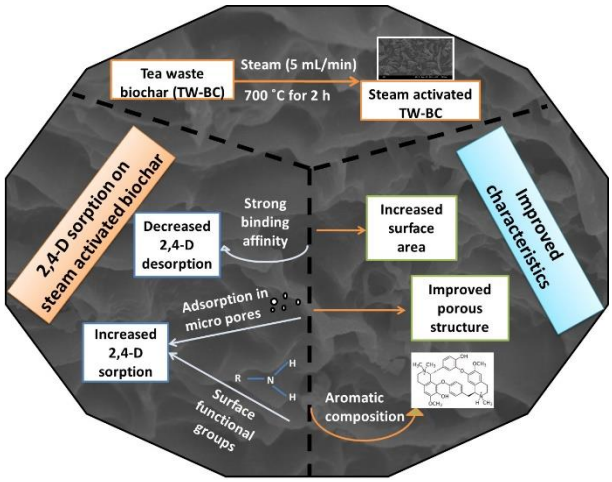

Abstract

Objective of this study was to investigate the mechanisms of 2,4-dichlorophynoxy acetic acid (2,4-D) sorption on biochar in aqueous solutions. Sorption isotherm, kinetics, and desorption experiments were performed to identify the role of biochars' feedstock and production conditions on 2,4-D sorption. Biochars were prepared from various green wastes (tea, burcucumber, and hardwood) at two pyrolytic temperatures (400 and 700˚C). The tea waste biochar produced at 700 ˚C was further activated with steam under a controlled flow. The sorption of 2,4-D was strongly dependent on the biochar properties such as specific surface area, surface functional groups, and microporosity. The steam activated biochar produced from tea waste showed the highest (58.8 mg g^{-1}) 2,4-D sorption capacity, which was attributed to the high specific surface area (576 m^2g^{-1}). The mechanism of 2,4-D removal from aqueous solution by biochar is mainly attributed to the formation of heterogeneous sorption sites due to the steam activation.

Keywords: 2,4-D, biochar, Pyrolysis, Physical activation, Sorption kinetics

1. Introduction

Agriculture activities, forestry, and maintenance of green spaces rely heavily on the use of herbicide to control weeds. The leaching and runoff from agricultural and forest land, deposition from the aerial application, and discharge of industrial wastewater to ground and surface water bodies have caused severe contamination of the environment by herbicides. Many herbicides are not easily biodegradable, and some are carcinogenic in nature, and as such represent a concerning source of environmental toxicant (Gupta et al., 2006). 2,4-dichlorophenoxy acetic acid (2,4-D) is one of the oldest and more widely used herbicides (Kearns et al., 2014). 2,4-D is a systemic herbicide widely employed to selectively control broadleaf weeds. According to world health organization (WHO), 2,4-D is categorized as a

substance of "possibly carcinogenic to humans" (Loomis et al., 2015). It is highly soluble in water (solubility 900 mg L^{-1}) in comparison to other organic micro-pollutants (e.g. pharmaceuticals and hydrocarbons). The p*Ka* value of the herbicide is 2.7. Due to these reasons, removing 2,4-D from polluted waters can be challenging. The herbicide is anionic in nature, which also makes it weakly retained by intrinsically negatively charged soil and subsurface particles (Hermosin et al., 2006). This enables 2,4-D to quickly reach to the groundwater which, in many countries, is a common source of drinking water.

The development of an efficient, easily accessible and inexpensive technology is required for the removal of 2,4-D and other anionic herbicide compounds from water. The application of locally generated and low-cost adsorbents in water treatment processes can be a possible solution to address this issue, especially for developing countries.

Carbon (C) based biomass such as biochar has been used extensively to reduce toxicity levels of different pollutants in the environment (Ahmad et al., 2014; Uchimiya et al., 2010). Biochar is a by-product of the thermal decomposition of various organic biomasses to produce bio-oil. This process occurs over a range of temperatures (200-800 ˚C) under nitrogen environment with a limited supply of oxygen (Lehmann & Joseph, 2009). In the recent years, biochar has created a broad research interests due to its surface properties, high surface area, pore volume, and pore diameter that make it a strong candidate for the removal of contaminants from soil and water bodies (Mandal et al., 2016). Furthermore, biochar has a range of oxygen-containing surface functional groups (e.g., carboxyl, phenolic, hydroxyls) which make this C-based material effective to interact with diverse types of environmental contaminants (Lehmann & Joseph, 2015).

However, biochar properties (surface area, pore size distribution, surface charge and functional groups) greatly depend on different parameters such as biomass sources, pyrolysis temperature, pyrolysis procedure and post-treatment processes of the product (Lehmann, 2007b; Lehmann et al., 2011). From an environmental protection perspective, enhanced

contaminant retention capacity, faster removal/sorption kinetics and low reversibility of the sorption process are the most desirable characteristics of biochar materials.

Previous studies investigated the prevention of herbicide mobility in the environment through biochar application. For example, Kearns et al. (2014) found that biochar prepared from woodchips (350-700 ˚C), bamboo (500-700 ˚C) and corncobs (600 ˚C) adsorbed a higher quantity of 2,4-D compared to a commercial activated carbon. Similarly, Lü et al. (2012) reported that biochar produced from rice straw at 350 ˚C reduced the mobile 2,4-D concentration (100-600 μmol L^{-1}) in soils by up to 45%. In their study Lü et al. (2012) also investigated the effect of different pyrolysis temperatures (200, 350 and 500 ˚C) on biochar pore properties, surface functional groups and the herbicide sorption capacity.

The current study hypothesized that the presence of a greater surface area due to the presence of microporous structure and aromaticity or functional groups like carbonyl C=O, hydroxyl O-H and carboxyl in biochar would increase its ability to adsorb 2,4-D from aqueous solutions. In addition to the study of Lü et al. (2012) reported above there are a few other studies available on the sorption of 2,4-D by biochar (Gupta et al., 2006; Kearns et al., 2014), but none of these reports has specifically focused on a systematic investigation of the effect of feedstock source and steam activation on biochar's characteristics and their role on 2,4-D sorption. Steam activation is included in this study as it has been reported that this process can increase the degree of microporosity in biochar (Downie et al., 2009). This study underpins the feasibility of using biochar for remediating of 2,4-D and other problematic pesticides.

2. Materials and methods

2.1. Reagents

2,4-D (Sigma-Aldrich, Australia) was dissolved in ultrapure water to prepare a 1000 mg L^{-1} stock solution. The pH of the stock solution was raised to 11 by dropwise addition of 1 N

111 sodium hydroxide (NaOH) to enhance the compound's solubility (Kearns et al., 2014). The
112 stock solution was then stored in a dark container in a cold room (4 ºC) for further use. The
113 stock solution was diluted in 20 mM phosphate buffer saline (PBS) at pH 7 to get the targeted
114 initial 2,4-D concentration of 100 mg L^{-1} for the kinetic sorption experiments. Similarly, six
115 working solutions of 2,4-D (10, 50, 100, 200, 400, and 500 mg L^{-1}) were also prepared in
116 PBS for conducting the sorption isotherm experiments.
117

118 **2.2. Biochar preparation**

119 Four different types of feedstock were used to prepare biochar in this study. They were tea
120 waste, burcucumber, oak wood and bamboo. Tea waste was collected from a tea factory after
121 tea leaf processing and washed several times in distilled to remove impurities. After washing
122 the material was air-dried, crushed and ground to <1 mm in particle size for biochar
123 preparation. Tea wastes were pyrolyzed at 700 ˚C with a heating rate of 7 ˚C min^{-1} for 2 h
124 using a modified N11/H Nabertherm (Germany) furnace (Ahmad et al., 2012; Rajapaksha et
125 al., 2014). Nitrogen flow rate was set to 5 mL min^{-1} throughout the pyrolyzation. For steam
126 activation, samples were treated with 5 mL min^{-1} of steam during the last 45 min of the 2 h
127 total holding time at the peak temperature (700 ˚C). After steam activation, samples were
128 allowed to cool inside the chamber to 30 ˚C and then the final weight was recorded. The
129 samples from tea waste with and without steam activation were termed as TW-BC and TW-
130 BCS, respectively.
131 Burcucumber (*Cucumis anguria*) plants were collected and dried in air, then in an oven at 60
132 ˚C for 24 h. After drying, samples were ground and passed through <1 mm sieve. Crushed
133 samples were pyrolyzed at 700℃ by following the same pyrolysis procedure used for tea
134 waste. This biochar was termed as burcucumber biochar (BU-BC).

Oakwood and bamboo feedstock were collected and pyrolyzed at 400 ˚C for 2 h using a muffle furnace. Heating rate and N_2 supply were as above. After pyrolyzation, produced biochars were termed as OW-BC and B-BC.

2.3. Surface characterization of biochar

The pH of the biochar samples was measured using a pH meter (smartCHEM-LAB Laboratory Analyzer) in deionized water (1:10 ratio, W/V) after agitation in the end over end shaker at 20 rpm for 2 h followed by 5 min of settling time. The electrical conductivity (EC) of biochars was also measured in the same suspension using an EC electrode (smartCHEM-LAB Laboratory Analyzer) following 12 h of sediment settling. The C and N contents of biochar samples were determined with a Leco TruMac CNS Analyzer (LECO Corporation, USA). Cation exchange capacity (CEC) of the biochar samples was measured using the method described by Zelazny et al. (1996).

Biochar surface functional groups were determined using a Fourier-transform infrared spectrometer (FT-IR; Frontier, PerkinElmer, UK) at the wavenumber range of 600 - 4000 cm^{-1} by potassium bromide (KBr) pellet method. Each pellet was scanned 32 times at the resolution of 0.4 cm^{-1}. Baseline corrected spectra were used to identify the representative peaks of functional groups based on published literature (software; Thermo Nicolet). X-ray photoelectron spectroscopy (XPS) analysis was performed using a XPS spectrometer (K-Alpha, Thermo Scientific, UK) with a monochromatic Al α-Alpha radiation source, and a spot size around 400 μm in diameter with a detection limit around 0.5-1.0%. Gaussian-Lorentzian sum function was used for the XPS spectra deconvolution by XPSPEAK41.

Biochar particles were also examined by field emission scanning electron microscope (FE-SEM; Hitachi S-4300, Japan) to identify the surface morphology. The specific surface area and pore volume were analyzed by the Brunauer–Emmett–Teller (BET) method at −196 °C using a Gemini 2380 Surface Area Analyzer. Pore diameter was further determined using a

gas sorption analyzer (NOVA-1200; Quantachrome Corp., Boynton Beach, FL, USA) (Ahmad et al., 2014).

2.4. 2,4-D sorption kinetics and isotherm

2,4-D sorption experiments were performed using a batch equilibrium method. The kinetic experiment was conducted in 250 mL Schott bottle by mixing 0.25 g of each biochar sample with 100 mL of 100 mg L^{-1} 2,4-D solution (in PBS). All the containers were wrapped with aluminum foil to maintain in darkness. The mixture was then agitated using an end-over-end shaker at room temperature (23 ± 1 ˚C) at 10 rpm for 72 h. Subsamples (2 mL) were taken from each bottle at different time intervals (0.25, 0.5, 1, 2, 3, 5, 7, 10, 16, 24, 36, 48, 60, and 72 h). Samples were filtered using 0.45 µm cellulose ester filters immediately after collection. The filtrates after appropriate dilution were analyzed to determine 2,4-D concentrations by a spectrophotometric method at 282 nm (Aksu & Kabasakal, 2004) on a UV-VIS-NIR-Spectrophotometer (UV-3600, Shimadzu, Japan).

Sorption isotherms were determined at a constant pH 7 maintained by using PBS. It was found that the PBS was sufficient to control pH within ±0.2 units after addition of biochar materials (Kearns et al., 2014). Six working solutions (10, 50, 100, 200, 400, and 500 mg L^{-1}) of 2,4-D were prepared as described above. Fifty mL centrifuge tubes were used for the isotherm experiment. The weights of tubes and lids were recorded before adding biochar and 2,4-D solutions, which was needed to calculate the entrapped liquid weight and associated 2,4-D concentration during desorption experiments as explained later. Exactly 0.05 g of each biochar sample was placed inside the centrifuge tube, and 20 mL of each of the 2,4-D working solutions was added to it. The samples were agitated at 10 rpm using an end-over-end shaker for 72 h at room temperature (23±1 ˚C). The equilibration time was decided from the sorption kinetic experiments. After equilibration samples were centrifuged at 2403-G for 15 min to get clear supernatants which were further filtered using 0.45 µm cellulose ester

187 filters. The concentration of 2,4-D in the aliquot was determined by a UV-VIS-NIR-
188 Spectrophotometer as explained earlier.
189 After removing the supernatant, the weight of tubes containing wet biochar sediments was
190 recorded (for calculating the entrapped liquid weight). All the sorption experiments were
191 conducted in duplicates. The labware used in this study did not sorb any 2,4-D.
192 To evaluate and compare the 2,4-D sorption capacity of different biochars, the experimental
193 data were fitted using both Freundlich and Langmuir sorption models. The respective
194 mathematical expressions of these models are provided as Supplementary Information (SI).
195 Similarly, the sorption kinetic data were fitted to various kinetic models such as parabolic
196 diffusion, elovich equation, pseudo-first order and pseudo-second order models. The
197 mathematical expressions of these models are also given in SI.
198

199 **2.5. 2,4-D desorption**

200 The desorption of 2,4-D was determined following sorption of a known volume and
201 concentration of the 2,4-D solution. Just after the sorption experiment, 20 mL deionized
202 water was added to the sediment in each tube. Samples were agitated at 10 rpm on an end-
203 over-end shaker for 24 h at room temperature (23±1 ˚C). The suspension was then
204 centrifuged at 2403-G for 15 min. Clear supernatants were further filtered using 0.45 µm
205 cellulose ester filter for 2,4-D analysis as stated above. The amount of 2,4-D which was
206 entrapped in the wet biochar sediment coming straight from the sorption experiment was
207 taken into consideration for calculating the respective desorption amount.
208

209 **2.6. Statistical analysis**

210 An analysis of variance (ANOVA) using SPSS software packages (IBM SPSS Statistics 23)
211 was performed on the data to analyze the 2,4-D sorption capacity of different biochar
212 samples. A post hoc t-test at 5% level of significance was also conducted to quantify the

significance difference between biochar samples. Variability of the data was expressed as the standard deviation (STDEV) and a *p* value of <0.05 was considered as statistically significant.

3. Results and discussion

3.1. Characterization of biochar samples

The key physicochemical characteristics of biochar samples are shown in Table 1. Biochar prepared from tea waste with steam activation (TW-BCS) had a higher pH (11.9) and CEC (15.9 $cmol_c\ kg^{-1}$) values compared to the other four biochars. Furthermore, BU-BC showed a higher EC value (1403 $\mu S\ m^{-1}$) than other biochars (Table 1).

[Table 1]

The BU-BC had a much lower surface area (2.3 $m^2\ g^{-1}$; pore volume: 0.008 cm^3g^{-1}) than all the other materials probably due to the lower volatile organic matter content in the burcucumber biomass than the other biomass. For example, the C content of BU-BC was very low compared to TW-BCS produced at the same temperature (Table 1). The BU-BC contains a high amount of mineral ash which does not produce a high surface area as organic material (Lehmann, 2007a). Even though feedstock characteristics is important, pyrolysis temperature also seems to have a prominent effect on the surface area of the products. For example, TW-BCS had an extremely high surface area and pore volume (576 m^2g^{-1}; 109 cm^3kg^{-1}) compared to TW-BC and biochars from other two sources. Ahmad et al. (2012) reported that biochar produced at 700 ˚C had much higher surface area than that produced at a lower temperature 300 ˚C, which reflects the temperature effect on opening up of pore spaces due to the removal of volatile organic matters. Another study by Kloss et al. (2012) also found that increasing temperature from 400 to 525 ˚C increased the surface area of wheat straw-derived biochar from 4.8 to 14.2 m^2g^{-1}.

Biochar usually contains a microporous structure with higher pore volume and defined pore diameter. It was observed in this study that the pore volume of steam activated tea-waste biochar was the highest (109 $cm^3 kg^{-1}$) compared to the non-activated biochar and products produced from other biomass sources. Azargohar and Dalai (2008) also found that the physical (steam) activation increased the total pore volume of biochar samples. Similarly, an increase in the pore diameter of the biochar samples was observed as a result of steam activation (Table 1). Steam activated biochar with a large number of micropores (0-2 nm), and pore volume as shown in Table 1 could thus provide an increased herbicide sorption capacity as compared to the non-activated product (Rajapaksha et al., 2016; Rajapaksha et al., 2014). The polar surface area of 2,4-D is 47 $Å^2$. The relationship between pore size/diameter and 2,4-D sorption was investigated in the previous study by Kearns et al. (2014). The authors reported that pyrolysis conditions that produced BET surface areas up to 400 m^2g^{-1} primarily generated micropores accessible to N_2, but not 2,4-D due to the size exclusion. However, pyrolysis conditions that produced surface areas between 400 to 600 m^2g^{-1} increased 2,4-D sorption with increasing surface area, indicating the progressive widening of micropores into the larger sized pores that accommodated 2,4-D molecules. In our study, we also found the increased surface area and pore diameter with steam activation of tea waste biochar. Moreover, these properties increased 2,4-D sorption by steam-activated biochar. Biochars produced at the higher temperature were highly carbonized and exhibited highly aromatic structures, which was shown by the FTIR data. The IR spectra showed the presence of C-H, C=O, carboxyl, phenolic and other oxygen-containing functional groups on biochar surfaces (Supplementary information).

The bands observed at 3446 cm^{-1} (TW-BC and TW-BCS) can be assigned to the hydroxyl (-OH) stretching vibration (Yaman, 2004). The hydroxyl groups might be decreased with steam activation due to the ignition loss of OH during the activation at high temperature (Yuan et al., 2011). Bands at 1567 and 1557 cm^{-1} represented the presence of strong nitro (N-O)

stretching vibration (Nakanishi, 1962). The presence of C=C and carbonyl (-COH) was observed at 1432 and 1431 cm^{-1}, and the intensity of these groups was increased after steam activation of the biochar (Hsu et al., 2009). The increased band intensity at 1384 cm^{-1} represented the presence of –COOH bending vibration in the steam activated biochar (Supplementary information). Bands at 874 and 875 cm^{-1} can be assigned to the aromatic C-H bending (Uchimiya et al., 2013) (Supplementary information). However, FTIR spectra did not show very significant differences between TW-BC and TW-BCS except demonstrating changes in the intensity of certain bands.

While FTIR data represented the bulk surface characteristics of biochar materials, XPS analysis aimed to identify the presence of specific functional groups, especially the O-containing functional groups. The O1s and C1s spectra of TW-BC and TW-BCS are presented in Fig. 1. The relative percentage of specific functional groups from O1s and C1s spectra are shown in the supplementary section. The XPS spectra showed that the O content of the steam-activated biochar (TW-BCS; O atom % = 21.04) was higher than the non-activated biochar (TW-BC; O atom % = 17.47). The peaks at binding energies of 531.3 and 531.9 eV were assigned to O=C and O-C functional groups. The relative intensity of O=C and O-C functional groups are significantly higher in TW-BCS (15.6 and 73.7%) compared to TW-BC (14.4 and 59.2%) (Fig. 1a and 1b). Moreover, the relative intensity of –COOH functional groups at a binding energy of 289.3 eV is only observed in TW-BCS (Fig. 1c and 1d; Supplementary information) (Liu et al., 2010). The XPS results confirmed that the steam activation could conserve a greater proportion of O-containing functional groups (e.g., –COOH as also indicated by FTIR spectra) when compared with the non-activated biochar prepared from the same feedstock.

[Figure 1]

The difference between CEC values also described the presence of effective functional groups on biochar surfaces. Previous studies found that increasing pyrolysis temperature

290 decreased the CEC value due to the loss of carboxyl functional groups during the pyrolysis
291 process (Gai et al., 2014). However, the current study demonstrated that the steam activated
292 biochar had the highest CEC value in comparison to other products (Table 1). Therefore,
293 biochars produced at a similar temperature but with steam activation might help to conserve
294 the oxygen-containing functional groups (like carboxyl), which would lead to a higher CEC
295 value. Harvey et al. (2011) also reported that the higher CEC value of biochar might reflect
296 the presence of a higher carboxylic group contents.
297 Scanning Electron Microscopic (SEM) images showed the morphological and structural
298 changes between TW-BC and TW-BCS (Supplementary information). High-resolution SEM
299 images (2000x) depicted more defined pore structure in TW-BCS compared to TW-BC. The
300 well-defined pore structure might have caused the greater surface area in the steam activated
301 biochar than the non-activated product (Azargohar & Dalai, 2008) (Table 1).
302
303 **3.2. Sorption of 2,4-D by biochar**
304 *3.2.1. . 2,4-D sorption kinetics*
305 Several kinetic models such as parabolic diffusion, elovich equation, pseudo-first order and
306 pseudo-second order models were tested in this study. The best kinetic model fitting was
307 determined by considering the estimated correlation coefficient (R^2) values, which was
308 highest for the pseudo-second order model (Table 2). Yao et al. (2011) found that the pseudo-
309 first order and second order models better described the phosphate removal data on biochar
310 compared to the elovich equation. All the other model parameters presented in the
311 supplementary information.
312 The sorption kinetic modeling allowed to calculate the sorption rate as well as explained the
313 possible reaction mechanisms by identifying suitable rate expression characteristics. The
314 sorption rate of 2,4-D was initially fast and then followed a slower sorption rate until
315 gradually approaching an equilibrium (Fig. 2). The initial faster sorption might attribute to a

316 large amount of pore spaces available for the sorption (Rajapaksha et al., 2016). The steam
317 activated biochar adsorbed 2,4-D more efficiently compared to the other products (Fig. 2).
318 The reason could be that the steam activation enhanced the pore volume and pore diameter
319 (Table 1) of biochar samples, which influenced the sorption process. Previous studies also
320 found similar results, for example, Lima et al. (2010) reported that steam activation could
321 increase the sorption ability of biochar by enhancing the pore diameter. Rajapaksha et al.
322 (2016) found that steam activation of biochar could increase the pore size from 1.75 to 1.99
323 nm, which consequently increased sulfamethazine sorption by the product.
324 [Figure 2]
325 The estimated kinetic parameters for the pseudo-second order model are shown in Table 2
326 and the parameters for the other models in supplementary information. The pseudo-first order
327 model could be more relevant when the initial adsorbate concentration was higher, and the
328 pseudo-second order model could be more applicable when the initial adsorbate
329 concentration was lower (Liu, 2008). The best-fitted pseudo-second order model in the
330 current study suggested that the sorption of 2,4-D on biochar was a function of the
331 availability of surface sorption sites (Zhang et al., 2012). Furthermore, the best fitness of
332 pseudo-second order model for 2,4-D sorption on biochar confirms that the sorption process
333 may be controlled by both the physical and chemical processes (Sarkar et al., 2010). The
334 pseudo-second order rate constant was increased from 0.04 in TW-BC to 0.21 in TW-BCS
335 (Table 2). The K (sorption constant) value for TW-BCS was higher than for the rest of the
336 four biochars (Table 2). This indicated that the sorption of 2,4-D on steam activated biochar
337 was faster than the non-activated product and biochar from other sources. The kinetic
338 sorption results of 2,4-D on biochar indicated that the feedstock composition and steam
339 activation played a key role in the sorption process. The kinetics of sorption of the biochars
340 followed the similar order of 2,4-D sorption capacities obtained from the sorption isotherm
341 calculations (section 3.2.2). The difference in sorption ability could greatly depend on the

342 biochar characteristics which are a function of biomass source and production technology
343 (Martin et al., 2012). In this study, biochar prepared at the same temperature but with steam
344 activation enhanced the specific characteristics (surface area, pore diameter, functional
345 groups, pH) of biochar, which led to an increased 2,4-D sorption capacity.
346 [Table 2]
347
348 3.2.2. *2,4-D sorption isotherm*
349 Two isothermal models such as Freundlich and Langmuir were tested to fit the sorption data.
350 The Freundlich model best described the data with R^2 values of up to 0.98 (Table 3). Zhang
351 et al. (2011) found that the sorption of simazine on biochar was best fitted to the Freundlich
352 isotherm model with high R^2 (>0.98) values. The lower n value from the Freundlich model
353 indicated the heterogeneous sorption domain in the sorbent and the presence of higher
354 sorption site energy distribution (Pignatello & Xing, 1995). The fitting parameters for all
355 attempted models are shown in the supplementary information.
356 [Figure 3]
357 Fig. 3 represents the Freundlich isotherms for the sorption of 2,4-D to five biochar samples.
358 The steam activated biochar had the highest sorption capacity (58.8 mg g^{-1}) with moderate n
359 and high K and R^2 values, compared to the other four biochars. The best 2,4-D sorption
360 fitness with Freundlich model compared to Langmuir model suggests the formation of more
361 heterogeneous sorption sites on biochar because of the steam activation (Rusmin et al., 2015).
362 In general, 2,4-D sorption capacity decreased in the order: TW-BCS>OW-BC>BU-BC>B-
363 BC>TW-BC. For TW-BC and TW-BCS, some nonlinearity was observed at low adsorbate
364 concentration, but the linearity increased with increasing 2,4-D concentrations. The high
365 sorption on TW-BCS might be attributed to the high surface area of the biochar. Previous
366 studies also supported our findings, for example, Ahmad et al. (2012) observed that biochar
367 prepared at a higher temperature with high surface area (448.2 m^2 g^{-1}) removed

368 trichloroethylene (TCE) more efficiently than that prepared at a lower temperature (300 ˚C;
369 surface area: 3.14 $m^2 g^{-1}$). Few authors also found that biochar with a lower surface area
370 could adsorb more 2,4-D than biochar with a higher surface area. For example, Lü et al.
371 (2012) found that biochar produced from rice straw at 300 ˚C (20.6 m^2g^{-1}) could adsorb 2,4-D
372 more than biochar at 500 ˚C (128 m^2g^{-1}). The reason could be the difference in the chemical
373 composition between the biochar samples which played an important role in increasing the
374 sorption capacity at low temperature despite having a lower surface area (Lü et al., 2012).
375 In order to better compare the sorption ability of biochar to those of other sorbents, the
376 sorption distribution coefficient (K_d) was calculated (Table 4). The K_d values were
377 normalized to organic carbon content (K_{oc}). The formula for K_d and K_{oc} is presented in the
378 supplementary information. Within the tested concentration ranges, the K_d value was on the
379 order of 10^3 (L kg^{-1}) for TW-BCS. The observed K_d values are much larger than those
380 reported in the previous studies for natural geo-sorbents, including soils (K_d<10 L kg^{-1}),
381 humic substances, and clay minerals (K_d<100 L kg^{-1}) (Ji et al., 2009) and less than those
382 recorded for black carbon (K_d<10^6 L kg^{-1}) (Teixidó et al., 2011). The K_d values of 2,4-D by
383 TW-BCS was significantly higher than biochar produced from other sources. Also, the
384 sorption studies showed a higher 2,4-D removal by TW-BCS than other biochar samples. The
385 reason could be attributed to the microporous nature, higher surface area and aromatic carbon
386 structure of the TW-BCS materials. Our findings are supported by previous research, such as
387 Ren et al. (2016) found that the sorption affinity of phenanthrene to biochar (700 ˚C) was
388 significantly higher than biochar (300 ˚C) because of microporous nature and higher surface
389 area of biochar (700 ˚C). Moreover, from Table 4 the increased K_{oc} value for TW-BCS was
390 also observed. K_{oc} values are useful to estimate the relative affinity and attraction of the
391 herbicide to the biochar materials. Therefore, it also predicts the herbicide mobility in the
392 solution (Futch & Singh, 1999). Higher K_{oc} values correlate with the greater sorption of 2,4-
393 D by biochar samples whereas lower K_{oc} values represent the higher mobility of 2,4-D in

394 solution (Buttler et al., 1991). Therefore, sorption of 2,4-D to steam activated biochar was
395 much higher compared to non-activated biochar due to having improved surface properties.
396 [Table 3]
397 [Table 4]
398 *3.2.3. 2,4-D desorption*
399 The sorbed 2,4-D by a single extraction with deionized water only removed 4.4 to 21.5% of
400 2,4-D that was sorbed. A maximum 21.5% of 2,4-D desorption was observed in the case of
401 TW-BC, whereas the lowest desorption was observed in the case of TW-BCS (4.4%). This
402 indicated that the steam activated biochar had a stronger binding affinity to 2,4-D compare to
403 other biochars. This also implied that biochar with steam activation held a lesser risk of
404 possible release of adsorbed 2,4-D into the environment. The reason could be the diffusion
405 process that might limit/decrease the desorption of 2,4-D from steam activated biochar (TW-
406 BCS) (Ahmad et al., 2012). Loganathan et al. (2009) observed that the herbicide atrazine
407 remained much higher (five times) in the char-amended soil after desorption and washing
408 steps compared to soil alone. Desorption of pesticides like carbofuran from biochar prepared
409 from red gum wood (*Eucalyptus* spp.) was also less than the control due to the strong
410 sorption of pesticide on biochar surface (Yu et al., 2009).
411
412 **4. Conclusions**
413 Results of this research demonstrated that the laboratory prepared biochars could adsorb 2,4-
414 D from solution. Sorption studies showed that the steam activated biochar adsorbed 2,4-D
415 more efficiently than its non-steam activated biochars. Due to having a higher surface area,
416 pore volume, and pore diameter the steam activated biochar showed a higher 2,4-D sorption
417 capacity. Furthermore, a reduced 2,4-D desorption indicated that the steam activated biochar
418 could also retain 2,4 D more efficiently. Future studies should focus more in detail on the

419 mechanism of herbicide sorption and retention of a range of activated biochars in comparison
420 to their conventionally prepared counterparts.
421
422 E-supplementary data for this work can be found in e-version of this paper online.
423
424 **Acknowledgments**
425 Sanchita Mandal is thankful to the Department of Education and Training, Government of
426 Australia, for awarding her an Australian Postgraduate Award (APA).
427
428 **Reference**
429 Ahmad, M., Lee, S.S., Dou, X., Mohan, D., Sung, J.-K., Yang, J.E., Ok, Y.S. 2012. Effects of
430 pyrolysis temperature on soybean stover- and peanut shell-derived biochar properties
431 and TCE adsorption in water. *Bioresource Technology*, **118**, 536-544.
432 Ahmad, M., Rajapaksha, A.U., Lim, J.E., Zhang, M., Bolan, N., Mohan, D., Vithanage, M.,
433 Lee, S.S., Ok, Y.S. 2014. Biochar as a sorbent for contaminant management in soil
434 and water: a review. *Chemosphere*, **99**, 19-33.
435 Aksu, Z., Kabasakal, E. 2004. Batch adsorption of 2, 4-dichlorophenoxy-acetic acid (2, 4-D)
436 from aqueous solution by granular activated carbon. *Separation and Purification*
437 *Technology*, **35**(3), 223-240.
438 Azargohar, R., Dalai, A.K. 2008. Steam and KOH activation of biochar: Experimental and
439 modeling studies. *Microporous and Mesoporous Materials*, **110**(2–3), 413-421.
440 Buttler, T., Hornsby, A., Tucker, D., Knapp, J., Noling, J. 1991. Citrus: managing pesticides
441 for crop production and water quality protection: a supplement to the IFAS pest
442 control guides. *Circular-Florida Cooperative Extension Service (USA)*.
443 Cao, X., Ma, L., Gao, B., Harris, W. 2009. Dairy-manure derived biochar effectively sorbs
444 lead and atrazine. *Environmental Science & Technology*, **43**(9), 3285-3291.

445 Chakravarty, S., Dureja, V., Bhattacharyya, G., Maity, S., Bhattacharjee, S. 2002. Removal
446 of arsenic from groundwater using low cost ferruginous manganese ore. *Water*
447 *research*, **36**(3), 625-632.
448 Downie, A., Crosky, A., Munroe, P. 2009. Physical properties of biochar. *Biochar for*
449 *environmental management: Science and technology*, 13-32.
450 Futch, S., Singh, M. 1999. Herbicide mobility using soil leaching columns. *Bulletin of*
451 *environmental contamination and toxicology*, **62**(5), 520-529.
452 Gai, X., Wang, H., Liu, J., Zhai, L., Liu, S., Ren, T., Liu, H. 2014. Effects of feedstock and
453 pyrolysis temperature on biochar adsorption of ammonium and nitrate. *PloS one*,
454 **9**(12), e113888.
455 Gerente, C., Lee, V., Cloirec, P.L., McKay, G. 2007. Application of chitosan for the removal
456 of metals from wastewaters by adsorption—mechanisms and models review. *Critical*
457 *Reviews in Environmental Science and Technology*, **37**(1), 41-127.
458 Gupta, V.K., Ali, I., Suhas, Saini, V.K. 2006. Adsorption of 2,4-D and carbofuran pesticides
459 using fertilizer and steel industry wastes. *Journal of Colloid and Interface Science*,
460 **299**(2), 556-563.
461 Harvey, O.R., Herbert, B.E., Rhue, R.D., Kuo, L.-J. 2011. Metal interactions at the biochar-
462 water interface: energetics and structure-sorption relationships elucidated by flow
463 adsorption microcalorimetry. *Environmental science & technology*, **45**(13), 5550-
464 5556.
465 Hermosin, M., Celis, R., Facenda, G., Carrizosa, M., Ortega-Calvo, J., Cornejo, J. 2006.
466 Bioavailability of the herbicide 2, 4-D formulated with organoclays. *Soil biology and*
467 *Biochemistry*, **38**(8), 2117-2124.
468 Hsu, N.-H., Wang, S.-L., Liao, Y.-H., Huang, S.-T., Tzou, Y.-M., Huang, Y.-M. 2009.
469 Removal of hexavalent chromium from acidic aqueous solutions using rice straw-
470 derived carbon. *Journal of hazardous materials*, **171**(1), 1066-1070.

471 Inyang, M., Gao, B., Ding, W., Pullammanappallil, P., Zimmerman, A.R., Cao, X. 2011.
472 Enhanced lead sorption by biochar derived from anaerobically digested sugarcane
473 bagasse. *Separation Science and Technology*, **46**(12), 1950-1956.
474 Ji, L., Chen, W., Zheng, S., Xu, Z., Zhu, D. 2009. Adsorption of sulfonamide antibiotics to
475 multiwalled carbon nanotubes. *Langmuir*, **25**(19), 11608-11613.
476 Kearns, J.P., Wellborn, L.S., Summers, R.S., Knappe, D.R.U. 2014. 2,4-D adsorption to
477 biochars: Effect of preparation conditions on equilibrium adsorption capacity and
478 comparison with commercial activated carbon literature data. *Water Research*, **62**, 20-
479 28.
480 Kloss, S., Zehetner, F., Dellantonio, A., Hamid, R., Ottner, F., Liedtke, V., Schwanninger,
481 M., Gerzabek, M.H., Soja, G. 2012. Characterization of slow pyrolysis biochars:
482 effects of feedstocks and pyrolysis temperature on biochar properties. *Journal of*
483 *environmental quality*, **41**(4), 990-1000.
484 Lehmann, J. 2007a. Bio-energy in the black. *Frontiers in Ecology and the Environment*, **5**(7),
485 381-387.
486 Lehmann, J. 2007b. A handful of carbon. *Nature*, **447**(7141), 143-144.
487 Lehmann, J., Joseph, S. 2009. *Biochar for environmental management: science and*
488 *technology*. Earthscan.
489 Lehmann, J., Joseph, S. 2015. *Biochar for environmental management: science, technology*
490 *and implementation*. Routledge.
491 Lehmann, J., Rillig, M.C., Thies, J., Masiello, C.A., Hockaday, W.C., Crowley, D. 2011.
492 Biochar effects on soil biota - A review. *Soil Biology and Biochemistry*, **43**(9), 1812-
493 1836.
494 Lima, I.M., Boateng, A.A., Klasson, K.T. 2010. Physicochemical and adsorptive properties
495 of fast-pyrolysis bio-chars and their steam activated counterparts. *Journal of chemical*
496 *technology and biotechnology*, **85**(11), 1515-1521.

497 Liu, S., Sun, J., Huang, Z. 2010. Carbon spheres/activated carbon composite materials with
498 high Cr (VI) adsorption capacity prepared by a hydrothermal method. *Journal of*
499 *hazardous materials*, **173**(1), 377-383.
500 Liu, Y. 2008. New insights into pseudo-second-order kinetic equation for adsorption.
501 *Colloids and Surfaces A: Physicochemical and Engineering Aspects*, **320**(1), 275-278.
502 Loganathan, V.A., Feng, Y., Sheng, G.D., Clement, T.P. 2009. Crop-residue-derived char
503 influences sorption, desorption and bioavailability of atrazine in soils. *Soil Science*
504 *Society of America Journal*, **73**(3), 967-974.
505 Loomis, D., Guyton, K., Grosse, Y., El Ghissasi, F., Bouvard, V., Benbrahim-Tallaa, L.,
506 Guha, N., Mattock, H., Straif, K., IARC, L. 2015. Carcinogenicity of lindane, DDT,
507 and 2, 4-dichlorophenoxyacetic acid. *The Lancet. Oncology*, **16**(8), 891.
508 Lü, J., Li, J., Li, Y., Chen, B., Bao, Z. 2012. Use of rice straw biochar simultaneously as the
509 sustained release carrier of herbicides and soil amendment for their reduced leaching.
510 *Journal of agricultural and food chemistry*, **60**(26), 6463-6470.
511 Mandal, S., Sarkar, B., Bolan, N., Ok, Y.S., Naidu, R. 2016. Enhancement of chromate
512 reduction in soils by surface modified biochar. *Journal of environmental*
513 *management*.
514 Martin, S.M., Kookana, R.S., Van Zwieten, L., Krull, E. 2012. Marked changes in herbicide
515 sorption–desorption upon ageing of biochars in soil. *Journal of Hazardous Materials*,
516 **231–232**, 70-78.
517 Nakanishi, K. 1962. Infrared absorption spectroscopy, practical.
518 Pignatello, J.J., Xing, B. 1995. Mechanisms of slow sorption of organic chemicals to natural
519 particles. *Environmental Science & Technology*, **30**(1), 1-11.
520 Rajapaksha, A.U., Vithanage, M., Lee, S.S., Seo, D.-C., Tsang, D.C.W., Ok, Y.S. 2016.
521 Steam activation of biochars facilitates kinetics and pH-resilience of sulfamethazine
522 sorption. *Journal of Soils and Sediments*, **16**(3), 889-895.

523 Rajapaksha, A.U., Vithanage, M., Zhang, M., Ahmad, M., Mohan, D., Chang, S.X., Ok, Y.S.
524 2014. Pyrolysis condition affected sulfamethazine sorption by tea waste biochars.
525 *Bioresource technology*, **166**, 303-308.
526 Ren, X., Yuan, X., Sun, H. 2016. Dynamic changes in atrazine and phenanthrene sorption
527 behaviors during the aging of biochar in soils. *Environmental Science and Pollution*
528 *Research*, 1-10.
529 Rusmin, R., Sarkar, B., Liu, Y., McClure, S., Naidu, R. 2015. Structural evolution of
530 chitosan–palygorskite composites and removal of aqueous lead by composite beads.
531 *Applied Surface Science*, **353**, 363-375.
532 Sarkar, B., Xi, Y., Megharaj, M., Krishnamurti, G.S.R., Rajarathnam, D., Naidu, R. 2010.
533 Remediation of hexavalent chromium through adsorption by bentonite based
534 Arquad® 2HT-75 organoclays. *Journal of Hazardous Materials*, **183**(1–3), 87-97.
535 Teixidó, M., Pignatello, J.J., Beltrán, J.L., Granados, M., Peccia, J. 2011. Speciation of the
536 ionizable antibiotic sulfamethazine on black carbon (biochar). *Environmental science*
537 *& technology*, **45**(23), 10020-10027.
538 Uchimiya, M., Lima, I.M., Thomas Klasson, K., Chang, S., Wartelle, L.H., Rodgers, J.E.
539 2010. Immobilization of heavy metal ions (CuII, CdII, NiII, and PbII) by broiler litter-
540 derived biochars in water and soil. *Journal of Agricultural and Food Chemistry*,
541 **58**(9), 5538-5544.
542 Uchimiya, M., Orlov, A., Ramakrishnan, G., Sistani, K. 2013. In situ and ex situ
543 spectroscopic monitoring of biochar's surface functional groups. *Journal of Analytical*
544 *and Applied Pyrolysis*, **102**, 53-59.
545 Wang, S., Gao, B., Li, Y., Mosa, A., Zimmerman, A.R., Ma, L.Q., Harris, W.G., Migliaccio,
546 K.W. 2015. Manganese oxide-modified biochars: Preparation, characterization, and
547 sorption of arsenate and lead. *Bioresource Technology*, **181**, 13-17.

548 Wang, X.S., Chen, L.F., Li, F.Y., Chen, K.L., Wan, W.Y., Tang, Y.J. 2010. Removal of Cr
549 (VI) with wheat-residue derived black carbon: reaction mechanism and adsorption
550 performance. *Journal of hazardous materials*, **175**(1), 816-822.
551 Yaman, S. 2004. Pyrolysis of biomass to produce fuels and chemical feedstocks. *Energy*
552 *conversion and management*, **45**(5), 651-671.
553 Yao, Y., Gao, B., Inyang, M., Zimmerman, A.R., Cao, X., Pullammanappallil, P., Yang, L.
554 2011. Removal of phosphate from aqueous solution by biochar derived from
555 anaerobically digested sugar beet tailings. *Journal of Hazardous Materials*, **190**(1-3),
556 501-507.
557 Yu, X.-Y., Ying, G.-G., Kookana, R.S. 2009. Reduced plant uptake of pesticides with biochar
558 additions to soil. *Chemosphere*, **76**(5), 665-671.
559 Yuan, J.-H., Xu, R.-K., Zhang, H. 2011. The forms of alkalis in the biochar produced from
560 crop residues at different temperatures. *Bioresource Technology*, **102**(3), 3488-3497.
561 Zelazny, L.W., He, L., Vanwormhoudt, A. 1996. Charge analysis of soils and anion
562 exchange. *Methods of Soil Analysis Part 3—Chemical Methods*(methodsofsoilan3),
563 1231-1253.
564 Zhang, G., Zhang, Q., Sun, K., Liu, X., Zheng, W., Zhao, Y. 2011. Sorption of simazine to
565 corn straw biochars prepared at different pyrolytic temperatures. *Environmental*
566 *Pollution*, **159**(10), 2594-2601.
567 Zhang, M., Gao, B., Yao, Y., Xue, Y., Inyang, M. 2012. Synthesis, characterization, and
568 environmental implications of graphene-coated biochar. *Science of the Total*
569 *Environment*, **435-436**, 567-572.
570
571

572 **Figures**

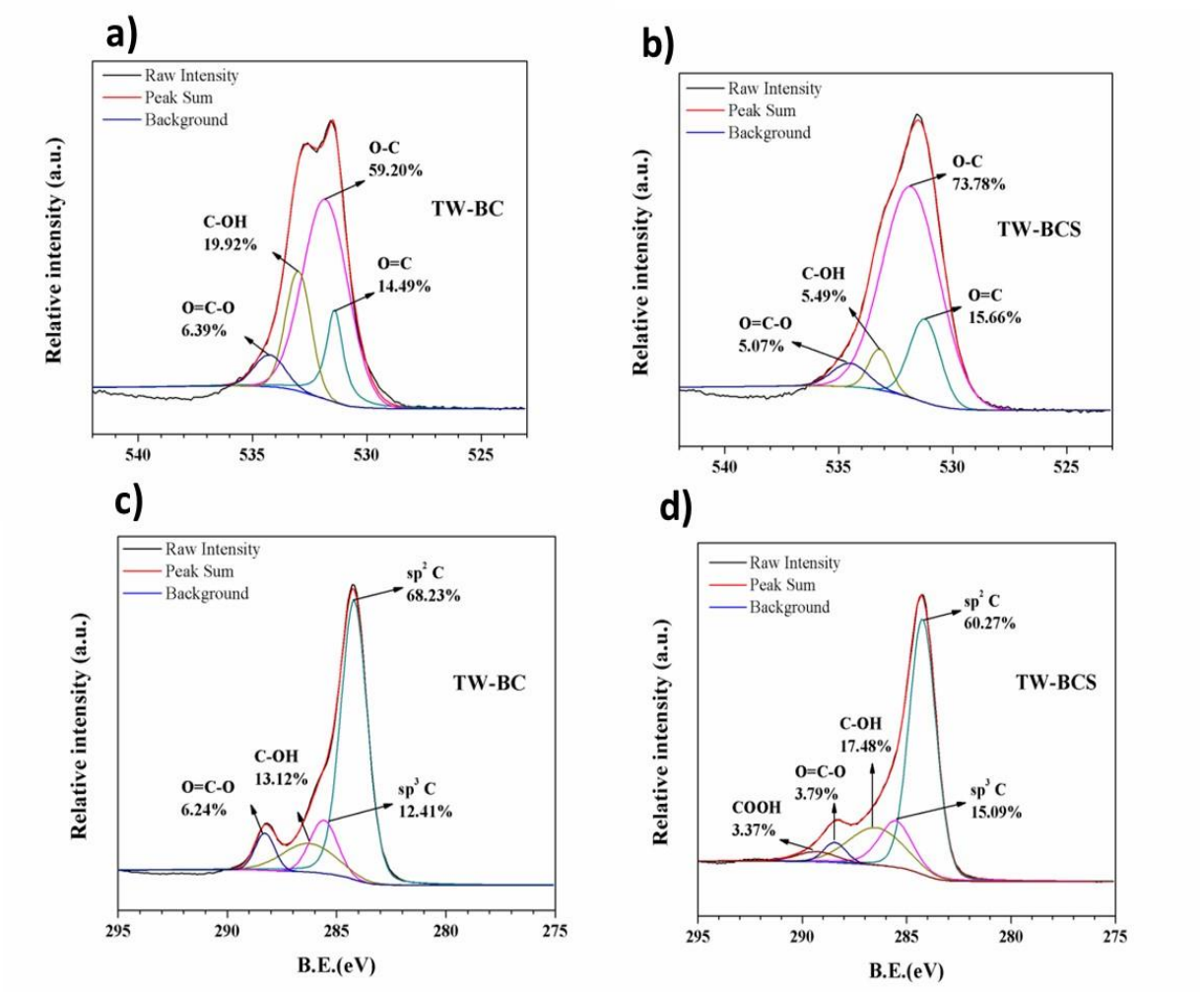

573

574

575

576 Figure 1: X-ray photoelectron spectroscopy (XPS) spectra of biochar samples: (a) O1 spectra

577 for TW-BC, (b) O1 spectra for TW-BCS, (c) C1s spectra for TW-BC, and (d) C1s spectra for

578 TW-BCS

579 *TW-BC: Tea waste biochar; TW-BCS: Steam activated tea waste biochar*

580

581

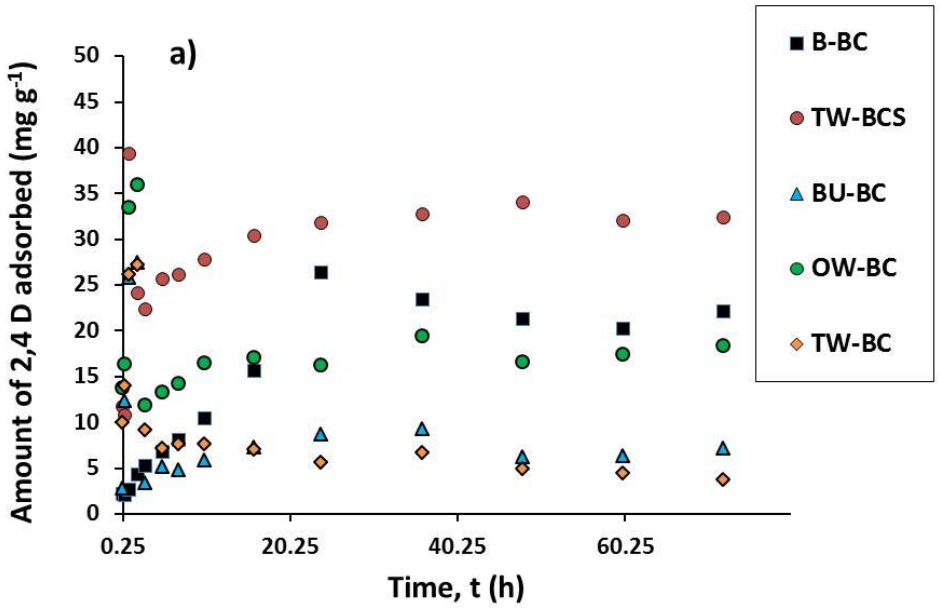

582

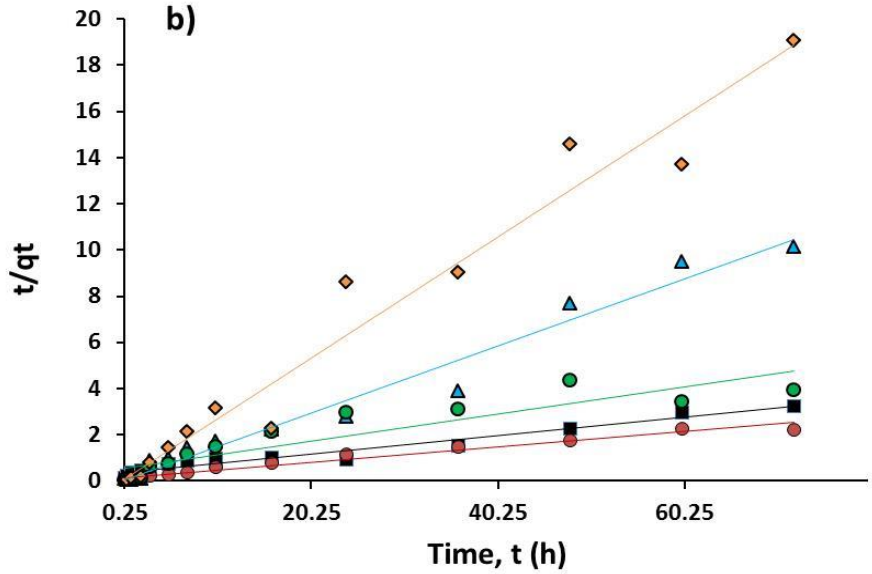

583

584 Figure 2: 2,4-D sorption kinetics on tea waste biochar (TW-BC), steam activated steam waste
585 biochar (TW-BCS), burcucumber biochar (BU-BC), oak wood biochar (OW-BC) and
586 bamboo biochar (B-BC) (a) sorption data; (b) amount of 2,4-D sorbed at time t (t/qt) (pseudo-
587 second order kinetic model fitting)

588

589

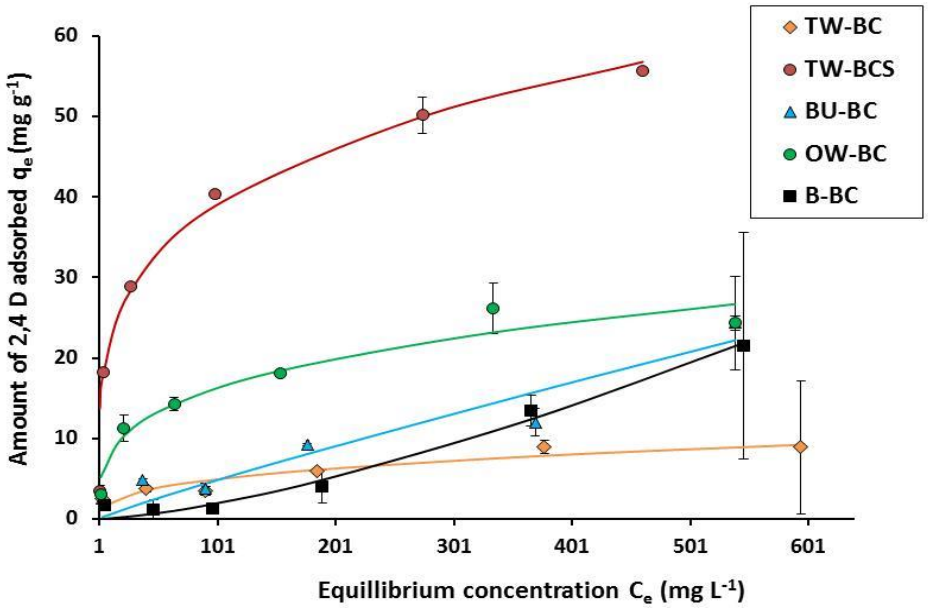

590

591 Figure 3: 2,4-D sorption isotherms on tea waste biochar (TW-BC), steam activated steam

592 waste biochar (TW-BCS), burcucumber biochar (BU-BC), oak wood biochar (OW-BC) and

593 bamboo biochar (B-BC) with Freundlich model fitting. Error bars represent the standard

594 deviation

595

596 **Tables**

597 Table 1: Physicochemical properties of five different biochar samples. Pore diameter and pore volume data were collected from Rajapaksha et al.

598 (2014) and Vithanage et al. (2015)

Sample name	**Pyrolysis temperature (˚C)**	**pH**	**EC (µS m^{-1})**	**CEC ($cmol_c$ kg^{-1})**	**C%**	**N%**	**Surface area (m^2 g^{-1})**	**Pore volume (cm^3 kg^{-1})**	**Pore diameter (nm)**
TW-BC	700	10.8±0.06	62.7±0.35	2.3±0.15	72.8±0.25	3.7±0.09	421.3	57.6	1.9
TW-BCS	700	11.9±0.02	221.4±0.25	15.9±1.16	63.4±0.73	3.4±0.07	576.1	109.1	2.0
BU-BC	700	10.7±0.12	1403.3±0.21	2.5±5.29	43.8±0.19	3.2±0.01	2.3	8.4	0.7
OW-BC	400	10.4±0.22	73.7±0.31	2.6±0.31	84.3±0.57	0.8±0.03	270.7	120.0	1.1
B-BC	400	10.2±0.23	24.9±0.41	3.6±0.75	86.2±0.12	0.6±0.03	475.6	209.0	1.1

599 *TW-BC: Tea waste biochar; TW-BCS: Steam activated tea waste biochar; BU-BC: Burcucumber biochar; OW-BC: Oak wood biochar; B-BC:*

600 *Bamboo biochar; EC: Electrical conductivity; CEC: Cation exchange capacity; ± indicates the standard deviation (STD) values*

601

602 Table 2: Fitted parameters values of sorption kinetic model (Pseudo-second order model)

Biochar	**Pseudo-second order model parameters**		
	Q_t Amount of 2,4-D adsorbed at time t (mg g^{-1} min^{-1})	K_2 (sorption constant)	R^2
TW-BCS	71.50	0.21	0.96
TW-BC	50.42	0.04	0.99
BU-BC	27.62	0.09	0.98
OW-BC	39.52	0.02	0.95
B-BC	2.68	0.17	0.96

603 *TW-BC: Tea waste biochar, TW-BCS: Steam activated tea waste biochar, BU-BC:*

604 *Burcucumber biochar, OW-BC: Oak wood biochar, and B-BC: Bamboo biochar; Kinetic*

605 *models are presented in the supplementary information*

606

607 Table 3. Freundlich and Langmuir model parameters for sorption isotherm of 2,4-D on

608 biochar

Biochar	**Freundlich model parameter**		
	K (sorption constant)	N (slope of sorption isotherm)	R^2
TW-BC	3.52	0.06	0.98
TW-BCS	3.63	0.75	0.98
BU-BC	0.22	0.30	0.85
OW-BC	2.23	0.39	0.94
B-BC	0.08	0.21	0.76
Biochar	**Langmuir model parameter**		
	K_f (sorption constant)	Q (maximum sorption capacity mg g^{-1})	R^2
TW-BC	0.02	10.05	0.96
TW-BCS	0.01	58.85	0.97
BU-BC	0.02	42.67	0.74
OW-BC	0.02	26.66	0.90
B-BC	0.04	28.92	0.71

609 *TW-BC: Tea waste biochar, TW-BCS: Steam activated TW-BC, BU-BC: Burcucumber*

610 *biochar, OW-BC: Oak wood biochar, B-BC: Bamboo biochar. Isotherm models are*

611 *expressed in the supplementary information*

612

613 Table 4: Distribution sorption coefficient (K_d and K_{oc}) of 2,4-D sorption for biochar samples

Biochar sample	**K_d (L kg^{-1})**	**K_{oc} (L kg^{-1})**
TW-BC	148.27	203.67
TW-BCS	1452.51	2291.02
BU-BC	155.72	355.53
OW-BC	404.68	480.05
B-BC	73.70	157.17

614 *Tea waste biochar (TW-BC), steam activated tea waste biochar (TW-BCS), burcucumber*

615 *biochar (BU-BC), oak wood biochar (OW-BC), and bamboo biochar (B-BC)*

616

Supplementary information:

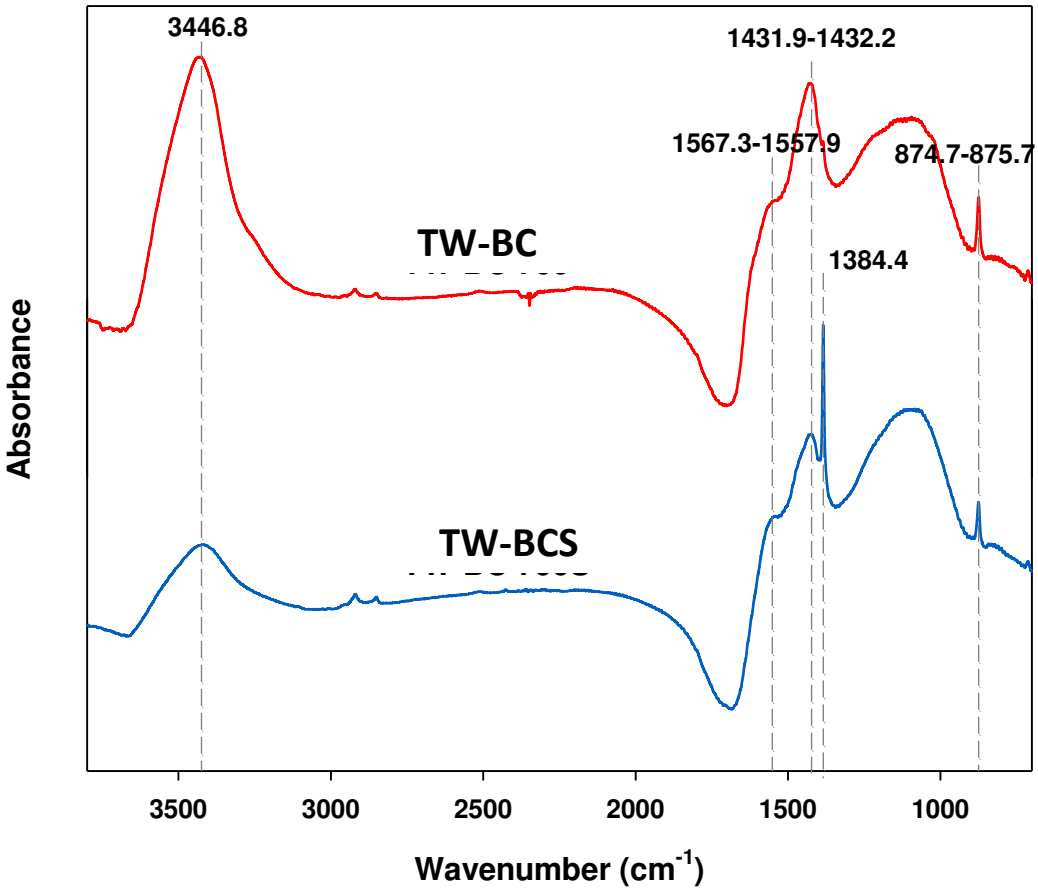

Figure 1: Fourier transform infrared spectroscopy (FTIR) spectrum to confirm the presence of functional groups on TW-BC (Tea waste biochar) and TW-BCS (steam activated tea waste biochar)

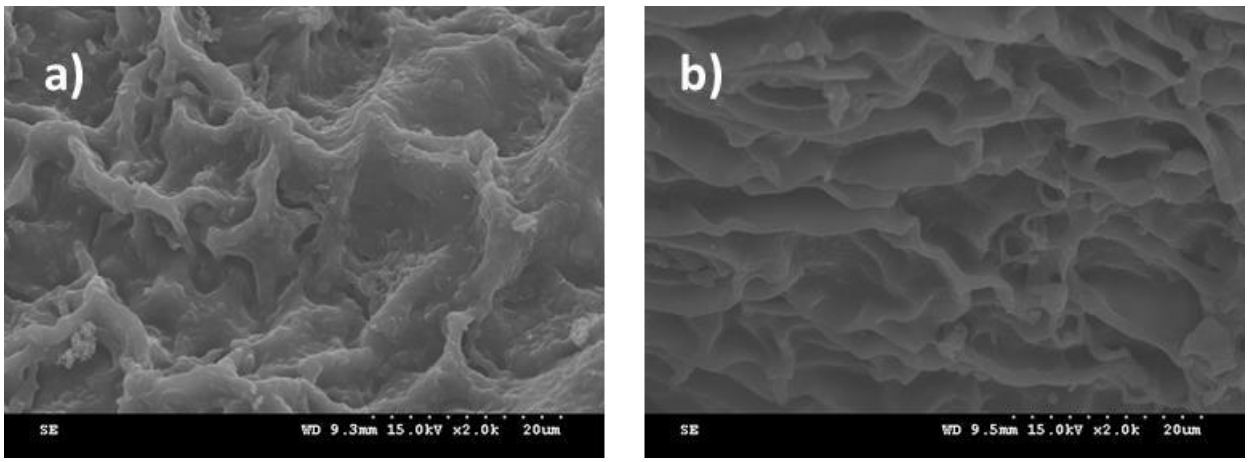

Figure 2: Scanning Electron Microscope (SEM) images of the surface of biochar: (a) tea waste biochar (TW-BC), and (b) steam activated tea waste biochar (TW-BCS)

Sorption models:

2,4-D sorption kinetic models were fitted by Parabolic diffusion, Elovich, Pseudo-first order and Pseudo-second order models. The respective equation can be expressed as follows (Wang et al., 2015; Yao et al., 2011)

Parabolic diffusion model

$$Q_t = A + R \times t^{1/2} \quad Eq.1$$

Elovich model

$$Q_t = \frac{1}{\beta} In(\alpha\beta) + \frac{1}{\beta} In(t) \quad Eq.2$$

Pseudo-first order model

$$Ln(Q_{e_1} - Q_t) = Ln(Q_{e_1} - K_1 t) \quad Eq.3$$

Pseudo-second order model

$$^{t}/_{Q_t} = 1(K_2^2 Q_{e_2}^2) + {}^{t}/_{Q_{e_2}} \quad Eq.4$$

Where, Where, q_t= amount of 2,4-D adsorbed at time t (mg $g^{-1}min^{-1}$), A = is the initial sorption rate (mg $g^{-1}min^{-1}$), α, β and R= Parabolic and Elovich model sorption constant, q_{e_1} and q_{e_2}= sorption capacity at equilibrium (mg g^{-1}) for Pseudo first order and second order, K_1 and K_2 = pseudo-first and second order constant and t = is the time (min). The Pseudo-first order and second order models describe the kinetics of the solid-solution based mononuclear and binuclear sorption respectively while considering the sorbent capacity (Gerente et al., 2007; Wang et al., 2010). Parabolic diffusion and Elovich models are empirical equations considering the contribution of desorption.

Sorption isotherm data were tested using Freundlich and Langmuir models, and the equations for the respective models can be written as follows (Yao et al., 2011)

Langmuir model

$$Q_e = \frac{K_f Q C_e}{1 + K_f C_e} \quad Eq.5$$

Freundlich model

$$Q_e = K C_e^n \quad Eq.6$$

Where, Q_e = Amount of 2,4-D adsorbed per unit weight of biochar samples (mg g^{-1}), Ce = the equilibrium concentration of the solution (mg L^{-1}), K_f and K = the Langmuir and Freundlich sorption constant, Q= Langmuir maximum sorption capacity (mg g^{-1}), n = slope of sorption isotherm. Langmuir model indicates the monolayer sorption into the homogeneous surface with no interaction between the adsorbed sorbent, while the Freundlich model is an empirical model often used to describe the chemisorption into the heterogeneous surface (Cao et al., 2009; Chakravarty et al., 2002; Inyang et al., 2011).

664 Table 1: Fitted parameters values of sorption kinetic models (Pseudo-first order model,

665 Parabolic diffusion model, and Elovich model)

Biochar	**Pseudo-first order model parameters**		
	Q_t Amount of 2,4-D adsorbed at time t (mg g^{-1} min^{-1})	K_1 (sorption constant)	R^2
TW-BCS	61.713	0.017	0.775
TW-BC	27.175	0.033	0.688
BU-BC	24.461	0.089	0.966
OW-BC	12.5698	0.018	0.664
B-BC	14.260	0.008	0.808
Biochar	**Parabolic diffusion model**		
	A Initial sorption rate (mg g^{-1} min^{-1})	R (sorption constant)	R^2
TW-BCS	7.483	3.011	0.825
TW-BC	5.855	46.025	0.694
BU-BC	2.818	4.979	0.951
OW-BC	1.477	33.807	0.523
B-BC	-2.117	26.743	0.721
Biochar	**Elovich model**		
	α sorption constant (mg g^{-1} min^{-1})	β (sorption constant)	R^2
TW-BCS	11.163	8.709	0.826
TW-BC	10.176	44.344	0.927
BU-BC	4.064	7.401	0.889

OW-BC	1.196	35.588	0.397
B-BC	-3.184	25.165	0.736

TW-BC: Tea waste biochar, TW-BCS: Steam activated tea waste biochar, BU-BC: Burcucumber biochar, OW-BC: Oak wood biochar, and B-BC: Bamboo biochar; Kinetic models are presented in the supplementary information

Distribution coefficient:

The sorption distribution coefficient (K_d) was calculated by,

$$K_d = \frac{Q_e}{C_e} \qquad Eq.7$$

Where, K_d = distribution coefficient (L kg^{-1}), Q_e = amount of 2,4-D adsorbed (mg kg^{-1}) and C_e = equilibrium concentration of 2,4-D (mg L^{-1})

Organic-carbon normalized K_d (K_{oc}) was calculated by,

$$K_{oc} = (K_d/\%C) \times 100 \quad Eq.8$$

Where, K_{oc}= distribution coefficient (L kg^{-1}), C= organic carbon content (%)

XPS analysis:

Table 2. Assignments of O1s and C1s characteristic peaks deconvoluted from XPS spectra (Liu et al., 2010) and its relative percentage in samples

Peak	Position (eV)	TW-BC	TW-BCS
O=C	531.3	22684.97	26429.98
O-C	531.9	92661.88	124493.60
C-OH	533.2	31181.91	9265.60
O=C-O	534.3	9999.22	8549.08

sp^2 C	284.2	207732.00	149724.40
sp^3 C	285.6	37783.74	37485.90
C-OH	286.3	39958.59	43424.45
O=C-O	288.3	19005.29	9404.57
COOH	289.3	0	8382.50

TW-BC: Tea waste biochar; TW-BCS: Steam activated tea waste biochar